Porosity Prediction from Seismic Attributes and Inversion

Philippe Ecoublet and William W. Symes *

December 1997

ABSTRACT

In complement to our study on fluid properties prediction using neural networks, this report focuses on the accuracy with which porosity can be inferred from different combinations of seismic parameters resulting from either prestack seismic inversion or the computation of poststack seismic attributes. This report also compares the prediction performance of the different neural networks introduced in previous reports.

Results from experiments conducted on synthetic data show that prestack inversion can improve porosity correlations by at least 30% over poststack seismic attributes. Also, poststack inversion little affects this performance with porosity correlations improved by 25% or so over poststack seismic attributes. Probabilistic neural networks performed better accuracy than traditional backpropagation neural networks achieving a gain in porosity correlation mostly superior to 10% over the backpropagation networks.

Introduction

In our initial phase of investigation of fluid properties prediction using a backpropagation neural network (Ecoublet, Symes and Levin, 1997), we established that relative fluctuations of elastic parameters are better correlated with fluid properties than absolute values. Training the network on relative fluctuations not only increases its generalization performance but also avoids empirical normalization of the data.

*The Rice Inversion Project, Department of Computational and Applied Mathematics, Rice University, Houston TX 77005-1892 USA, email ecoublet@caam.rice.edu

We noted that predicting from a large number of seismic attributes, some of which are poorly correlated with porosity, affects the generalization capabilities of the network defined with too many parameters, i.e. neurons.

Finally, we observed that the non-parametric probabilistic neural network achieves better porosity prediction from seismic inversion data, compared to the BPNN (Ecoublet and Symes, 1997).

The purpose of this report is to further investigate: 1) how seismic attributes can be combined to improve porosity prediction, 2) if porosity can effectively been infered from acoustic impedance alone.

The synthetic seismic data

As for the previous experiments, wells vaa58c and vaa58cst are chosen as training wells. The wells vaa56c and vaa55a are selected to test the network.

A 1D elastic model, built from the sonic log, V_p/V_s ratios from regional interpretation, and checkshot time-depth records, is used to generate synthetic offset seismograms using TRIP's visco-elastic modeling code. The modeling procedure is identical to the one described in (Ecoublet, Symes and Levin, 1997).

The linear fit, as a function of depth, of the elastic model is computed and constitutes the smooth background model. The residual relative fluctuations of the elastic parameters are used by the modeling code to compute the reflection coefficients. The seismic source is defined as a high frequency band-pass filter.

61 CMP traces are generated at 75ft offset spacing between 0 and 4500ft offset, and 1ms time sampling, at each well location. The synthetic seismograms are then inverted for the elastic parameters (ρ,V_p,V_s) as functions of depth. Details on the inversion procedure may be found in (Ecoublet, Symes and Levin, 1997). The impedance logs, Z_p and Z_s, are calculated for each well out of the inversion results.

The seismic attributes, defined in (Ecoublet, Symes and Levin, 1997), are calculated on the NMO corrected traces. A total of 27 attributes are computed from each NMO corrected trace and then summed to produce a single log for each attribute. The attribute logs are converted into depth and resampled at the sampling rate of the porosity log.

The CMP gathers are then stacked and the resulting stack converted into depth and resampled at 3ft sampling rate. The depth interval corresponding to the well logs interval is retained. The number of samples and depth intervals are given in Table 1 for each of the wells.

Well	Number of Samples
58c+st	591
56c	426
55a	347

Table 1. Summarize of data. Training wells: 58c and 58cst. Test wells: 56c and 55a.

The processing sequence detailed above is illustrated in Figure 1 with the synthetic seismograms generated at well 56c.

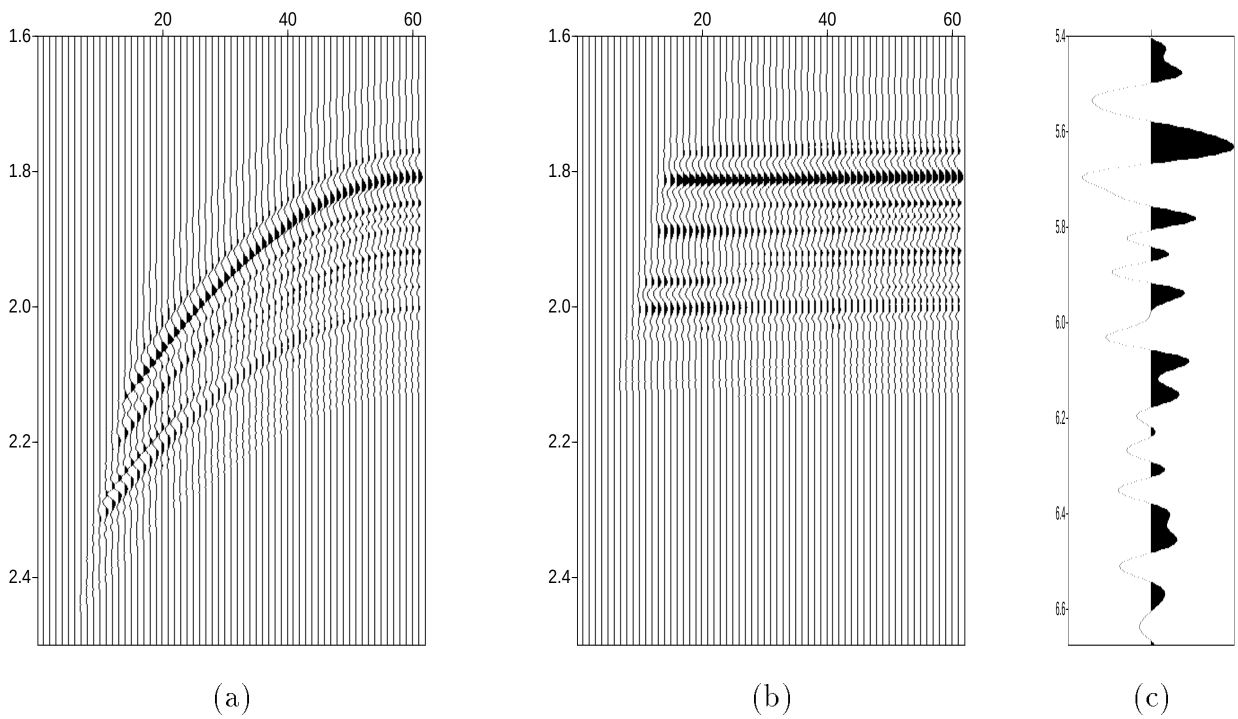

FIG. 1. (a) 61 CMP synthetic seismic traces generated at well 56c location. (b) nmo corrected seismograms. (c) stacked trace converted into depth within the log interval [5400ft,6675ft].

Correlation between porosity and seismic inversion

We observed in our initial report (Ecoublet, Symes and Levin, 1997) the higher correlation existing between relative fluctuations of seismic parameters and fluid properties at log scale, yielding better fluid properties prediction.

Relative fluctuation pseudo-logs are produced by subtracting the linear fit, as a function of depth, of the actual log. The correlation between fluid properties (ϕ,V_{sh},S_{wt}) and relative fluctuations of density, ρ, P-impedance, Z_p, and S-impedance, Z_s, were computed for each well and reported in Table 2 which also includes the correlation between fluids and the seismic stack.

We recall that the correlation coefficient used in our analysis, Cor_{xy}, is defined by

$$\mathrm{Cor}_{xy} = \frac{E((x-\overline{x})(y-\overline{y}))}{E((x-\overline{x})^2)^{\frac{1}{2}} E((y-\overline{y})^2)^{\frac{1}{2}}},$$

where $E()$ denotes the expected value function, $\overline{x}$ and $\overline{y}$ the mean of x and y respectively.

correlation coefficients (%)				
VAA58	seismic stack	ρ	Z_p	Z_s
ϕ	-45.85	-75.04	-67.41	-73.06
V_{sh}	43.30	72.06	67.02	68.13
S_w	25.17	47.35	45.55	42.62
VAA56	seismic stack	ρ	Z_p	Z_s
ϕ	-41.04	-72.40	-56.77	-72.45
V_{sh}	32.12	54.11	41.34	53.15
S_w	38.79	51.06	48.14	46.93
VAA55	seismic stack	ρ	Z_p	Z_s
ϕ	-59.70	-80.80	-77.09	-77.69
V_{sh}	59.12	78.47	75.24	76.88
S_w	51.86	72.37	72.08	64.11

Table 2. Correlation between seismic stack, relative fluctuations of ρ, Z_p, Z_s resulting from seismic inversion, and fluid properties at the different wells.

The correlation between relative fluctuations of seismic inversion results and fluid properties is very close to the log-to-log correlation observed between relative fluctuations of well logs and fluids, given in (Ecoublet, Symes and Levin, 1997), Table 9.

The density, P-impedance and S-impedance pseudo logs, and seismic stack are plotted against the porosity well log in Figures 2, 4 and 6 for wells vaa58, vaa56c and vaa55a respectively. The corresponding crossplots are shown in Figures 3, 5 and 7.

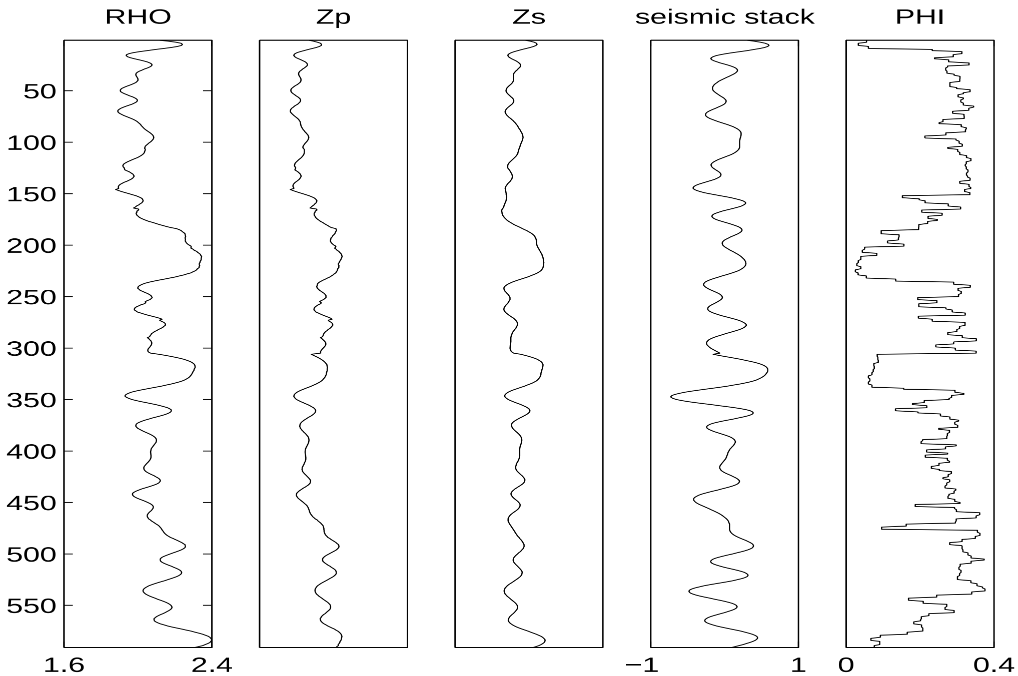

FIG. 2. (ρ, Z_p, Z_s) resulting from seismic inversion, seismic stack, and ϕ log for training wells 58c and 58cst. Vertical coordinates are in samples.

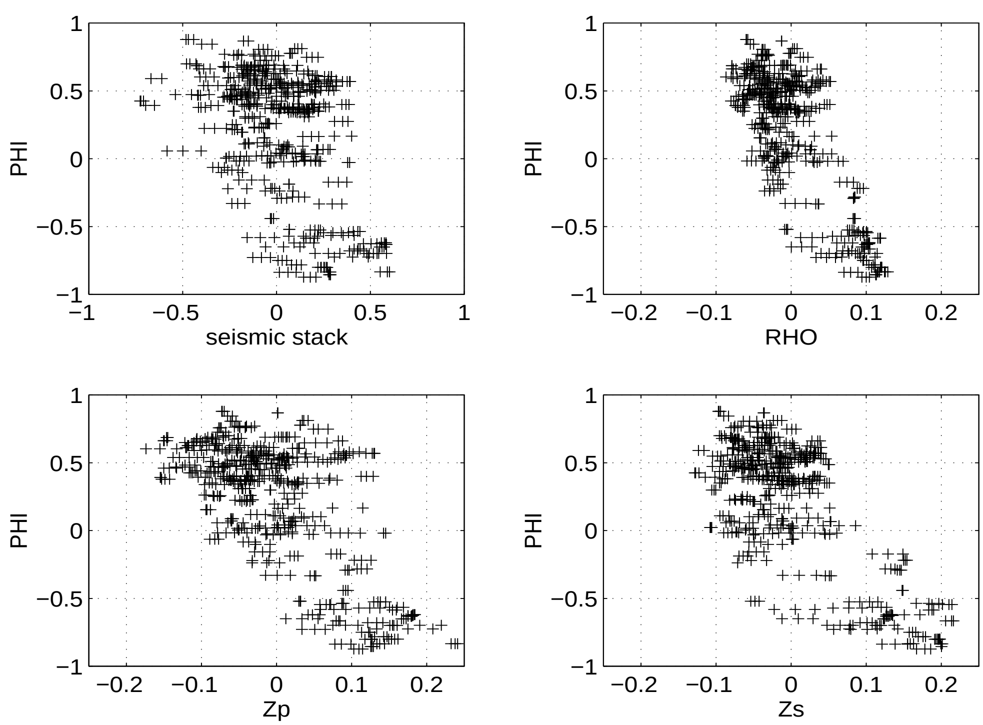

FIG. 3. Cross-plots between relative fluctuations of (ρ, Z_p, Z_s), seismic stack, and ϕ log for training wells 58c and 58cst.

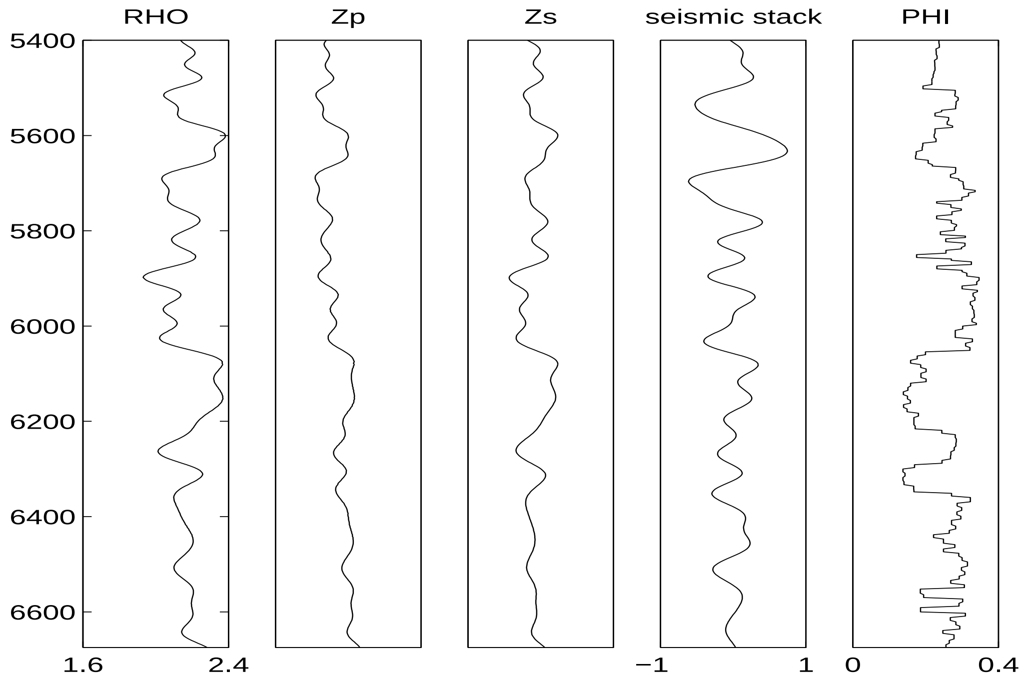

FIG. 4. (ρ, Z_p, Z_s) resulting from seismic inversion, seismic stack, and ϕ log for test well 56c. Vertical coordinates are in measured depth.

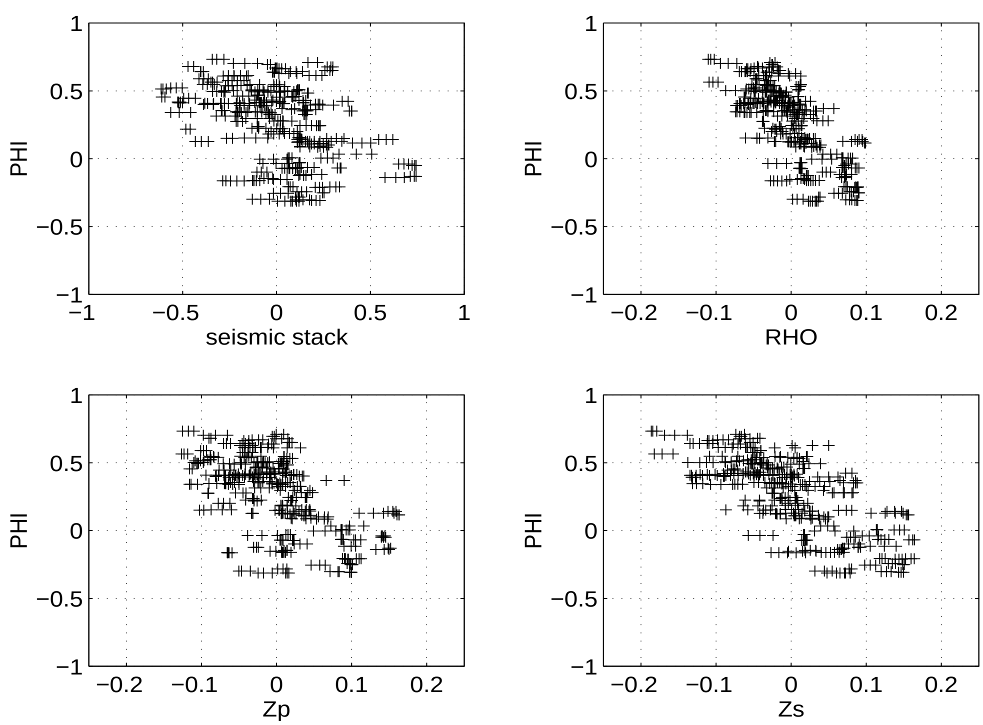

FIG. 5. Cross-plots between relative fluctuations of (ρ, Z_p, Z_s), seismic stack, and ϕ log for test well 56c.

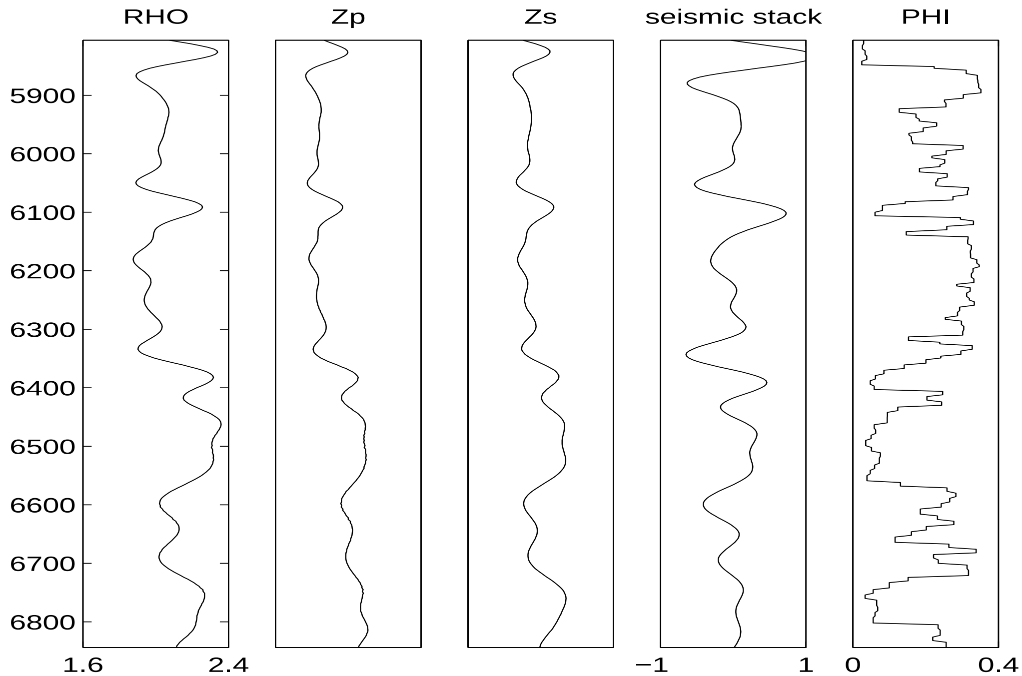

FIG. 6. (ρ, Z_p, Z_s) resulting from seismic inversion, seismic stack, and ϕ log for test well 55a. Vertical coordinates are in measured depth.

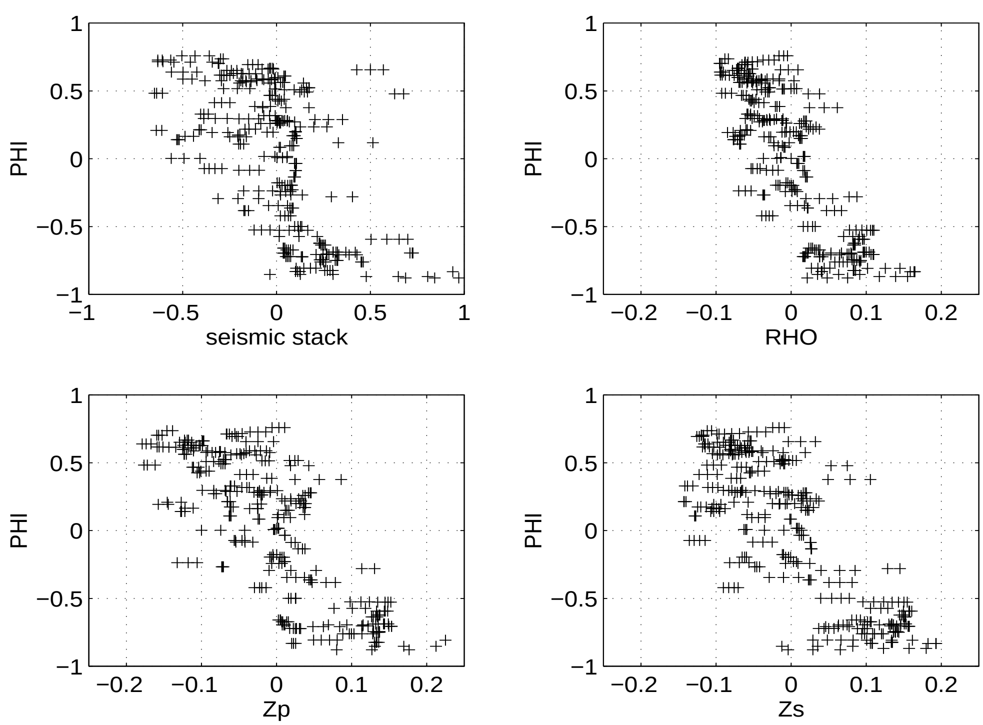

FIG. 7. Cross-plots between relative fluctuations of (ρ, Z_p, Z_s), seismic stack, and ϕ log for test well 55a.

Porosity prediction from seismic inversion

The backpropagation neural network in its prediction (BPNNp) and classification (BPNNc) version (Ecoublet, Symes and Levin, 1997) is implemented to infer porosity from seismic inversion. The probabilistic neural network (PNN) which has demonstrated superior results (Ecoublet and Symes, 1997), is also used and its performance compared to those of the backpropagation networks.

In the series of experiments described below we aim to assess the separate contribution of the density information, shear-wave impedance, and compressional-wave impedance in predicting porosity. To do so, we first predicted ϕ from (ρ, Z_p, Z_s), then dropped ρ from the input data, and finally estimated ϕ from Z_p only.

The parameterization of the BPNN is summarized in Table 3 for each case. As a common characteristic for all experiments, we constructed a BPNN with an hidden layer constituted of five neurons.

Network Parametererization			
predict ϕ from (ρ, Z_p, Z_s)	BPNNp	BPNNc	PNN
No. of input neurons	3×5	3×5	3
No. of output neurons	1	10	10
No. of weights	86	140	0
predict ϕ from (Z_p, Z_s)	BPNNp	BPNNc	PNN
No. of input neurons	2×5	2×5	2
No. of output neurons	1	10	10
No. of weights	61	115	0
predict ϕ from Z_p	BPNNp	BPNNc	PNN
No. of input neurons	1×5	1×5	1
No. of output neurons	1	10	10
No. of weights	36	90	0

Table 3. Characteristic of the neural networks built for different experiments.

The accuracy with which porosity is predicted, is measured by two quantities; the relative root mean square (rms) error, and a prediction coefficient, denoted C_p, defined by

$$C_p = \frac{T_\phi \cdot P_\phi}{||T_\phi||\ ||P_\phi||}.$$

Both rms error and prediction coefficient measure the match between the predicted porosity, P_ϕ, and targeted porosity, T_ϕ.

Porosity prediction from ρ, Z_p and Z_s

The results of porosity prediction from relative fluctuations of density, P and S-impedances, presented in (Ecoublet and Symes, 1997), are summarized in Table 4.

ϕ prediction error from ρ, Z_p and Z_s									
	BPNNp			BPNNc			PNN		
Well	rms$\times 10^2$	C_p%	Cor%	rms$\times 10^2$	C_p%	Cor%	rms$\times 10^2$	C_p%	Cor%
58	4.37	98.58	88.36	5.03	98.22	85.64	5.94	97.48	78.57
56	5.96	97.33	61.47	6.79	96.62	54.02	5.42	97.84	66.30
55	10.34	91.46	58.76	9.78	92.95	62.99	6.78	95.84	79.57

Table 4. Rms error and prediction coefficient between predicted and targeted ϕ from ρ, Z_p and Z_s resulting from seismic inversion.

The training porosity log is plotted in Figure 8 along with the estimated porosity obtained from using the prediction BPNN (BPNNp), the classification BPNN (BPNNc), and the PNN. Prediction of porosity from test data is illustrated in Figures 9 and 10. As we mentioned in (Ecoublet and Symes, 1997), the generalization capabilities of the BPNNp are affected by data normalization issues, especially in the case of well 55a. The best prediction in terms of minimum rms error and larger prediction coefficient is achieved with the probabilistic neural network.

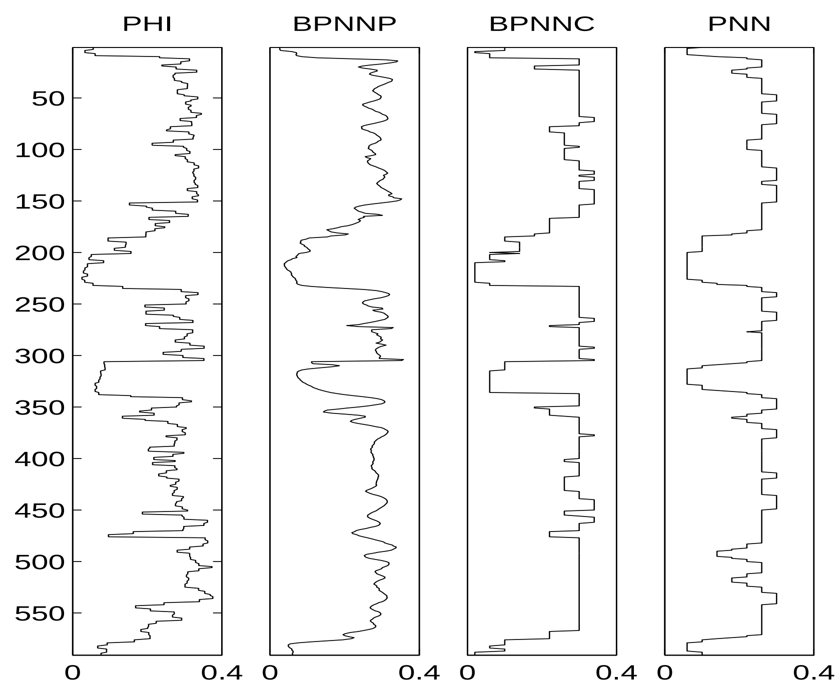

FIG. 8. ϕ predicted from ρ, Z_p, and Z_s resulting from seismic inversion. Prediction on training data from wells 58c and 58cst. Vertical coordinates are in samples.

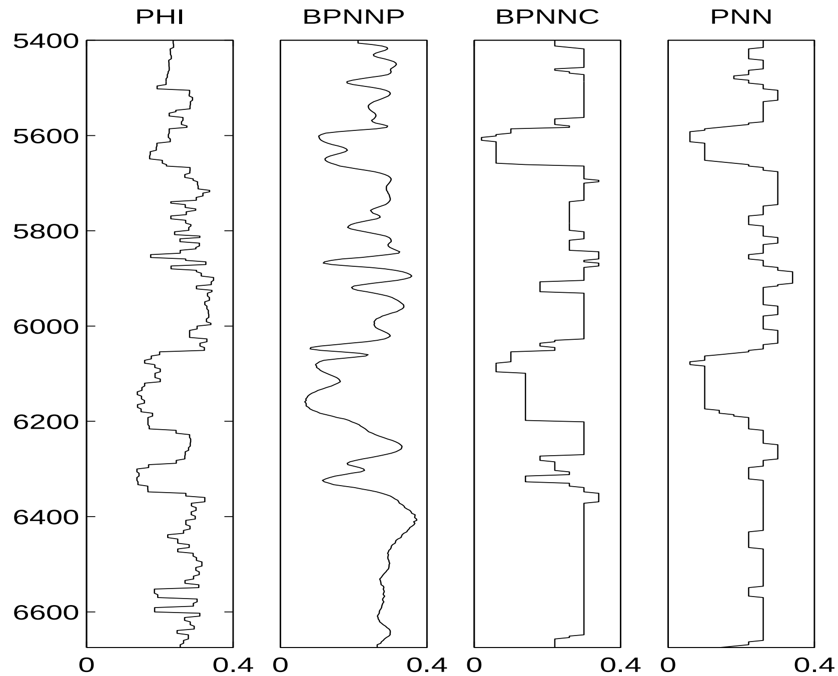

FIG. 9. ϕ predicted from ρ, Z_p, and Z_s resulting from seismic inversion, using the BPNNp, BPNNc and PNN. Prediction on test data from well 56c. Vertical coordinates are in measured depth.

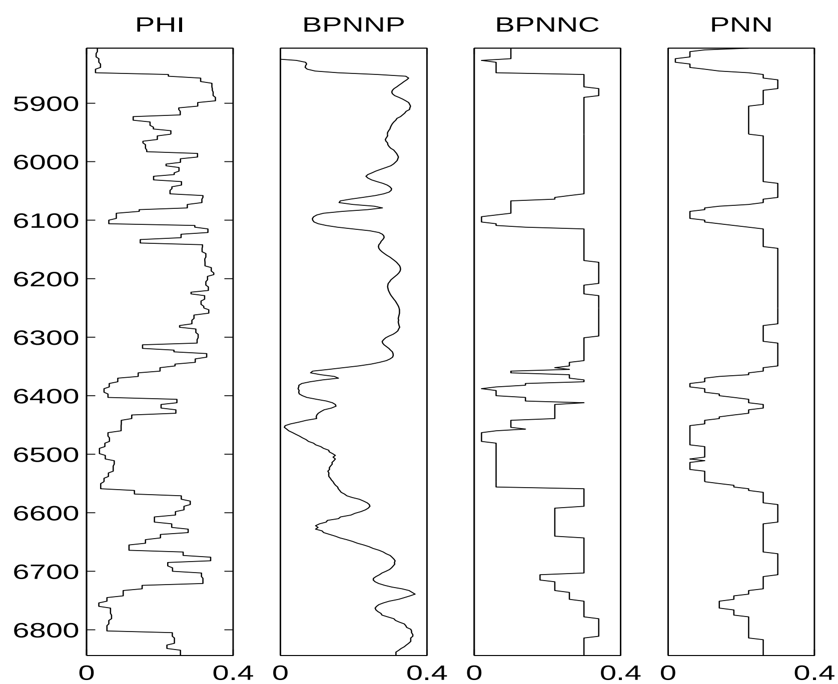

FIG. 10. ϕ predicted from ρ, Z_p, and Z_s resulting from seismic inversion, using the BPNNp, BPNNc and PNN. Prediction on test data from well 55a. Vertical coordinates are in measured depth.

Porosity prediction from Z_p and Z_s

We know estimate the porosity from only two quantities Z_p and Z_s. In general, porosity prediction is little affected by the absence of density information, in terms of residual errors, as shown in Table 5.

ϕ prediction error from Z_p and Z_s									
	BPNNp			BPNNc			PNN		
Well	rms$\times 10^2$	$C_p\%$	$Cor\%$	rms$\times 10^2$	$C_p\%$	$Cor\%$	rms$\times 10^2$	$C_p\%$	$Cor\%$
58	4.51	98.49	87.57	4.93	98.23	85.81	6.02	97.46	78.26
56	6.91	96.35	49.10	6.88	96.43	53.64	5.49	97.81	64.91
55	9.02	93.08	68.56	9.52	92.91	62.11	6.91	95.62	79.21

Table 5. Rms error and prediction coefficient between predicted and targeted ϕ from Z_p and Z_s resulting from seismic inversion.

The targeted and predicted porosity logs are plotted in Figure 11 for the training data, and in Figures 12 and 13 for the test data. In the absence of density information, the PNN performs almost as well, whereas the BPNN shows less robustness to a reduction in the input data, in particular in its prediction version.

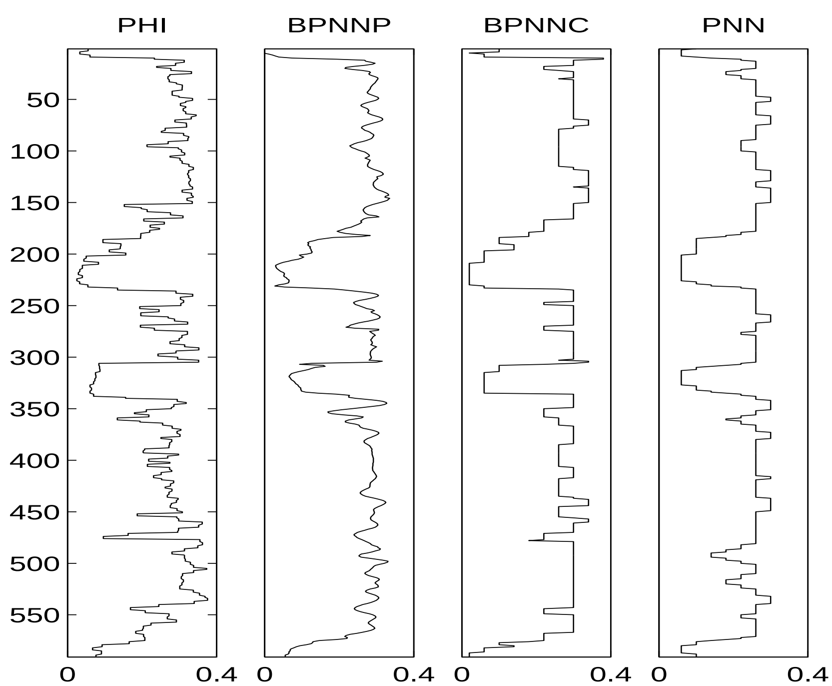

FIG. 11. ϕ predicted from Z_p and Z_s resulting from seismic inversion, using the BPNNp, BPNNc and PNN. Prediction on training data from wells 58c and 58cst. Vertical coordinates are in samples.

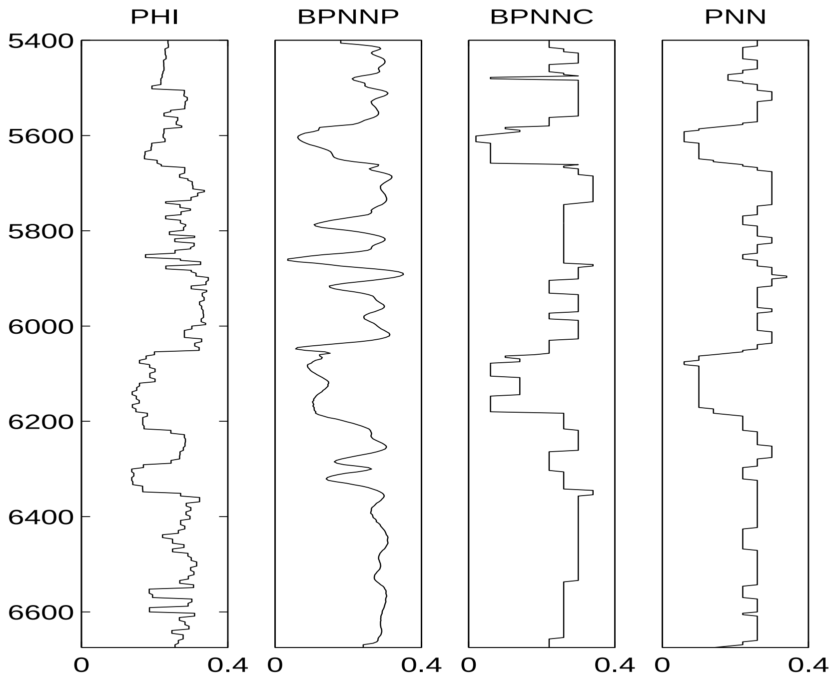

FIG. 12. ϕ predicted from Z_p and Z_s resulting from seismic inversion, using the BPNNp, BPNNc and PNN. Prediction on test data from well 56c. Vertical coordinates are in measured depth.

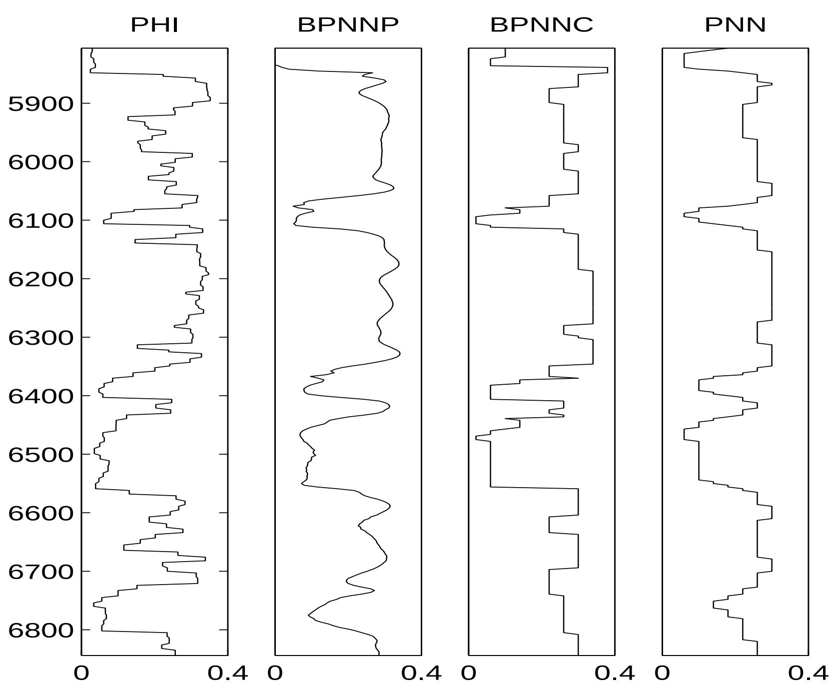

FIG. 13. ϕ predicted from Z_p and Z_s resulting from seismic inversion, using the BPNNp, BPNNc and PNN. Prediction on test data from well 55a. Vertical coordinates are in measured depth.

Porosity prediction from Z_p only

In this final experiment, porosity is predicted from Z_p only. The residual error of porosity prediction using the PNN increases steadily, as shown in Table 6. The evolution of the residual error and prediction coefficient achieved with the BPNN does not follow the same logical trend.

ϕ prediction error from Z_p only									
	BPNNp			BPNNc			PNN		
Well	rms$\times 10^2$	$C_p\%$	$Cor\%$	rms$\times 10^2$	$C_p\%$	$Cor\%$	rms$\times 10^2$	$C_p\%$	$Cor\%$
58	6.37	96.96	73.11	8.15	95.46	62.05	7.25	96.52	68.48
56	5.24	97.93	52.85	7.97	96.14	26.33	5.79	97.79	58.63
55	8.10	94.84	74.23	10.29	93.12	63.86	7.29	94.70	75.88

Table 6. Rms error and prediction coefficient between predicted and targeted ϕ from Z_p resulting from seismic inversion.

The porosity predicted from the training data (Figure 14) captures most of the features of the targeted log. The prediction results on the test data, plotted in Figures 15 and 16, shows that some of the low porosity zones are not recovered. Also the small scale variations are not predicted by the BPNN which produces a smooth response. A classification output will always appier blockier than a prediction output. In terms of resolution, there is no difference, however.

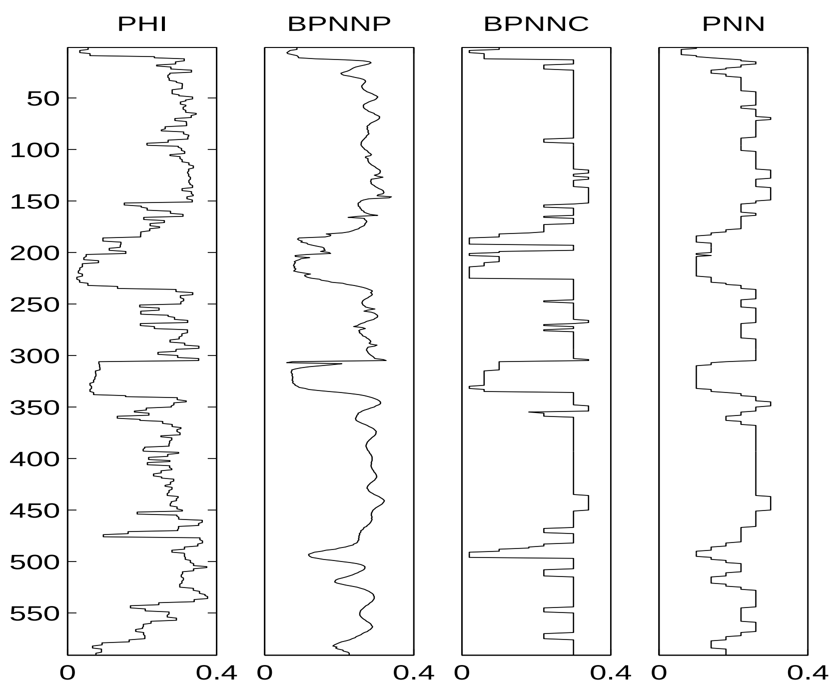

FIG. 14. ϕ predicted from Z_p resulting from seismic inversion. Prediction on training data from wells 58c and 58cst. Vertical coordinates are in samples.

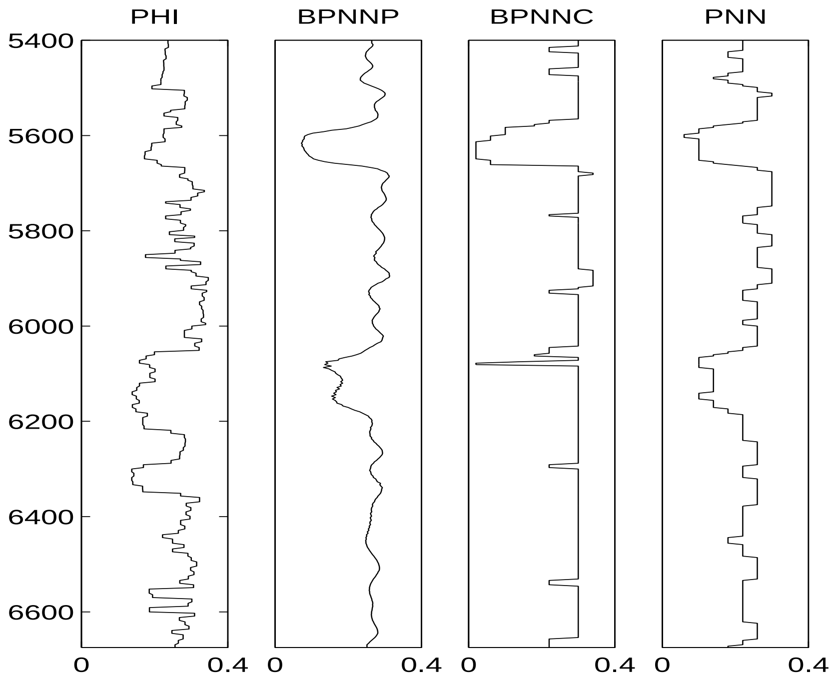

FIG. 15. ϕ predicted from Z_p resulting from seismic inversion, using the BPNNp, BPNNc and PNN. Prediction on test data from well 56c. Vertical coordinates are in measured depth.

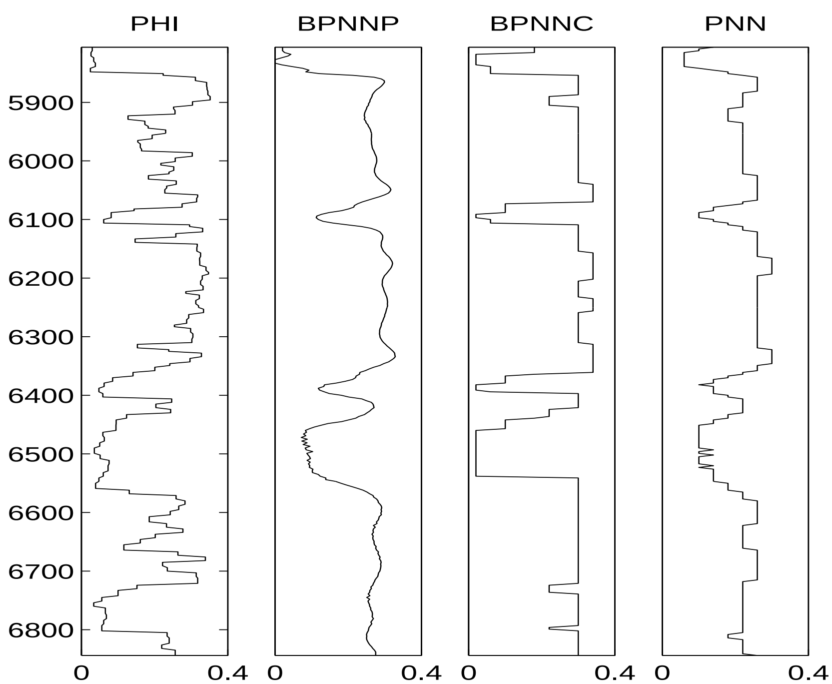

FIG. 16. ϕ predicted from Z_p resulting from seismic inversion, using the BPNNp, BPNNc and PNN. Prediction on test data from well 55a. Vertical coordinates are in measured depth.

The prediction results detailed in the previous section are summarized in Figure 17 in terms of rms error and correlation between targeted and predicted porosity from Z_p, i.e. one input log, (Z_p, Z_s), i.e. two input logs, and (ρ, Z_p, Z_s), i.e. three input logs.

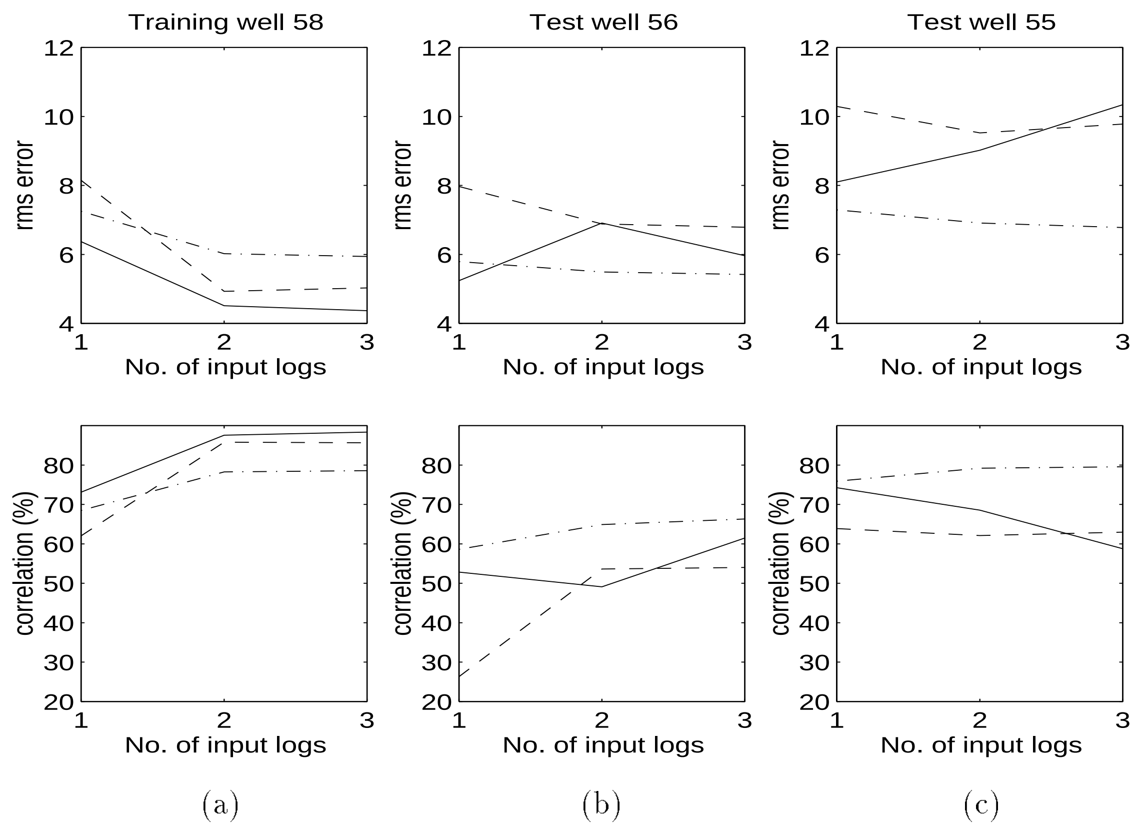

FIG. 17. (a) Rms error and correlation between targeted and predicted porosity at the training well 58 versus number of input logs of the neural network, using BPNNp (solid line), BPNNc (dashed line) and PNN (dotted line). (b) Rms error and correlation at the test well 56c, and (c) at the test well 55a.

The addition of the S-impedance information to the P-impedance reduces both the training and the prediction error, whereas the residual error does not significantly decrease when adding the density information.

The probabilistic network predicts porosity with the minimum rms error and the highest correlation with the targeted porosity.

Porosity prediction from seismic attributes

A total of 27 attributes listed in Table 7 and corresponding to class I and class III attributes (Taner *et al.*, 1979), were generated from the synthetic seismograms. Computed for each individual trace of the CMP gathers, each final attribute log is the result of the stack other the 61 traces. The correlation between each seismic attribute and porosity is also compiled in Table 7 for each well.

Class I attributes vs porosity - correlation coefficients (%)			
	$VAA58$	$VAA56$	$VAA55$
Real part of complex trace	-10.83	9.94	-19.75
Imaginary part of complex trace	-32.68	-34.65	-47.97
Trace envelope	-12.71	2.95	- 8.13
Time derivative of the envelope	- 0.32	-17.91	- 5.28
Second derivative of the envelope	- 0.27	2.12	6.59
Instantaneous phase	-24.70	-23.71	-40.05
Instantaneous frequency	15.31	-13.31	-22.39
Envelope weighted inst. freq.	31.11	-19.64	-28.24
Thin bed indicator	- 3.00	- 3.08	-14.57
Acceleration of phase	- 0.76	0.02	2.54
Dominant frequency	18.08	- 6.49	-27.13
Band width	13.59	11.10	- 6.70
Instantaneous Q factor	- 3.45	- 6.87	- 1.32
Normalized amplitude	- 3.02	2.86	- 9.59
Envelope amplitude modulated phase	-14.72	0.68	- 9.32
Relative acoustic impedance	-42.25	-37.14	-56.50
Class III attributes vs porosity - correlation coefficients (%)			
	$VAA58$	$VAA56$	$VAA55$
Trace envelope	-10.60	15.82	- 7.74
Time derivative of the envelope	-12.31	6.45	- 3.55
Second derivative of the envelope	- 7.20	9.16	-13.90
Instantaneous phase	-19.44	-19.06	10.82
Instantaneous frequency	20.18	- 0.60	- 8.14
Envelope weighted inst. freq.	21.49	- 4.09	-10.62
Acceleration of phase	-14.09	7.95	4.11
Dominant frequency	20.18	- 0.60	- 8.13
Band width	5.93	-10.30	14.34
Instantaneous Q factor	11.43	13.24	-16.51
Apparent polarity	-25.22	17.50	4.10

Table 7. Correlation coefficients between seismic attributes and porosity at each well

We differentiated the synthetic seismograms with respect to time in order to ensure compatibility between our model and Taner's model for the seismic data, i.e. the convolution of the source signature with the time derivative of relative variations of impedance.

Note that the results described in (Ecoublet, Symes and Levin, 1997) related to seismic attributes computation are erroneous. Consequently, the correlation coefficients given in (Ecoublet, Symes and Levin, 1997) Table 7 are wrong and should be discarded.

The imaginary part of complex trace attribute, very close to the seismic stack, shows a similar correlation with porosity. Similarly for the normalized amplitude attribute. The relative acoustic impedance is the best correlated attribute with porosity. Most of the other attributes are poorly correlated and show unconsistent correlations from well to well.

We compared porosity prediction from one, three and five selected attributes plotted in Figure 18 for the training well 58. First, we predicted porosity from a single attribute, the relative acoustic impedance. We then added the instantaneous phase and instantaneous frequency attributes, and finally trained the network with two additional attributes; the imaginary part of complex trace and instantaneous Q factor.

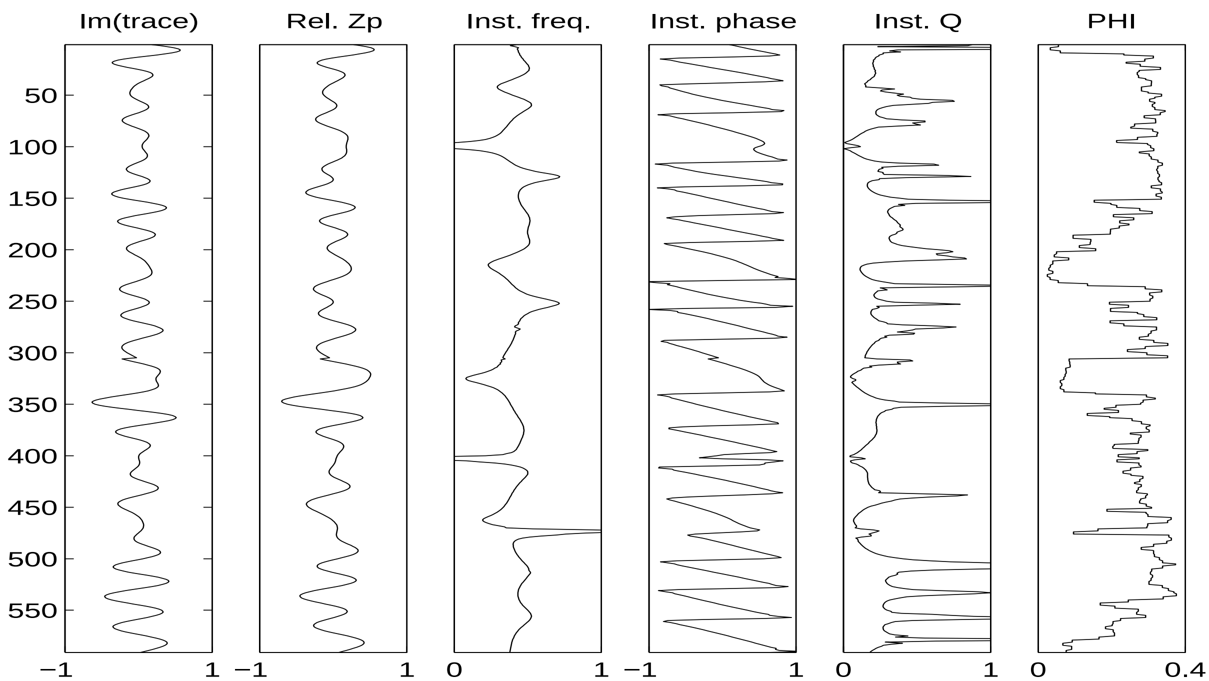

FIG. 18. Five selected seismic attributes versus porosity log at the training well 58; *imaginary part of complex trace*, *relative acoustic impedance*, *instantaneous frequency*, *instantaneous phase* and *instantaneous Q factor*.

Cross-plots between the seismic stack, the five selected attributes and porosity at the training well 58 (Figure 19) show the greater volatility existing between some attributes like instantaneous phase, instantaneous frequency, instantaneous Q factor, and porosity. It implies a lower correlation in spite of a significant clustering along linear trends.

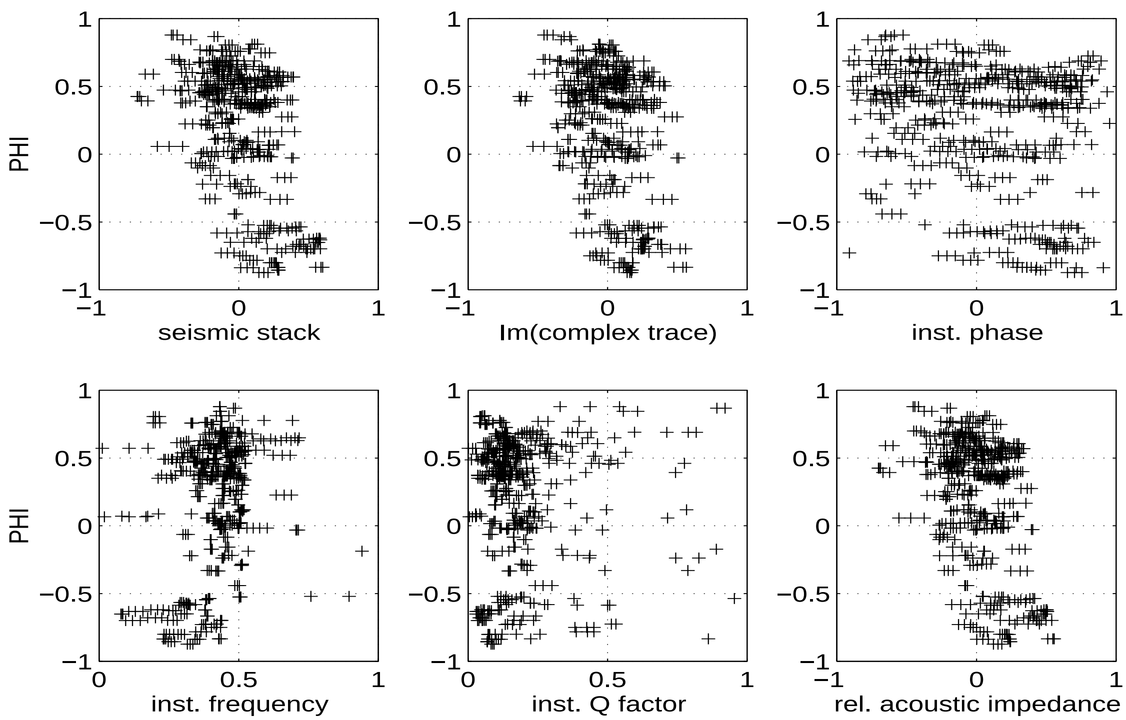

FIG. 19. Cross-plots between seismic stack, selected seismic attributes, and porosity log at the training well 58.

The prediction rms errors and prediction-target correlations obtained from the different combinations of seismic attributes are summarized in Figure 20.

The training error decreases as the number of attributes, and consequently the number of neurons constituting the network, increases. As a consequence of observed correlations, the error on test data increases with the number of attributes used to predict porosity.

These observations tend to show that the network overfits the training data by addition of attributes having a low correlation with porosity. In opposition, increasing the number of neurons affects the generalization capabilities of the network.

Note that the error of the BPNN in its prediction version follows a different trend due to predictions lying outside the range of the training data. Also, smaller residual errors are obtained when using the probabilistic network.

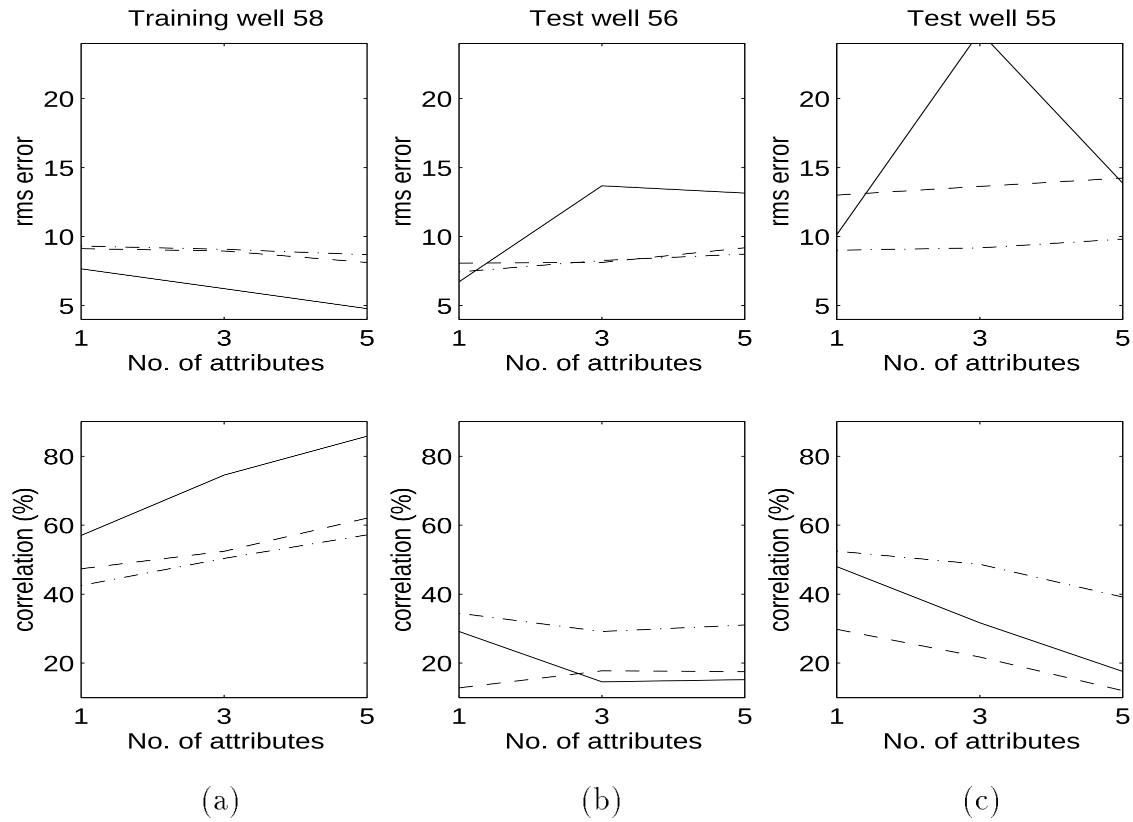

FIG. 20. (a) Rms error and correlation between targeted and predicted porosity at the training well 58 versus number of input attributes of the neural network, using BPNNp (solid line), BPNNc (dashed line) and PNN (dotted line). (b) Rms error and correlation at the test well 56c, and (c) at the test well 55a.

Results are detailed in Table 8 for porosity predicted from five seismic attributes. The predicted porosity logs obtained from the different networks are plotted in Figure 21 at the training well, and in Figures 22 and 23 at the test wells.

ϕ prediction error from five seismic attributes									
	BPNNp			BPNNc			PNN		
Well	rms$\times 10^2$	C_p%	Cor%	rms$\times 10^2$	C_p%	Cor%	rms$\times 10^2$	C_p%	Cor%
58	4.79	98.29	85.80	8.13	95.55	62.04	8.69	95.14	57.18
56	13.16	87.03	15.21	9.20	94.69	17.53	8.74	95.34	31.07
55	13.88	85.11	17.58	14.25	86.90	12.04	9.83	90.22	39.13

Table 8. Rms error, prediction coefficient and correlation between predicted and targeted ϕ from five seismic attributes.

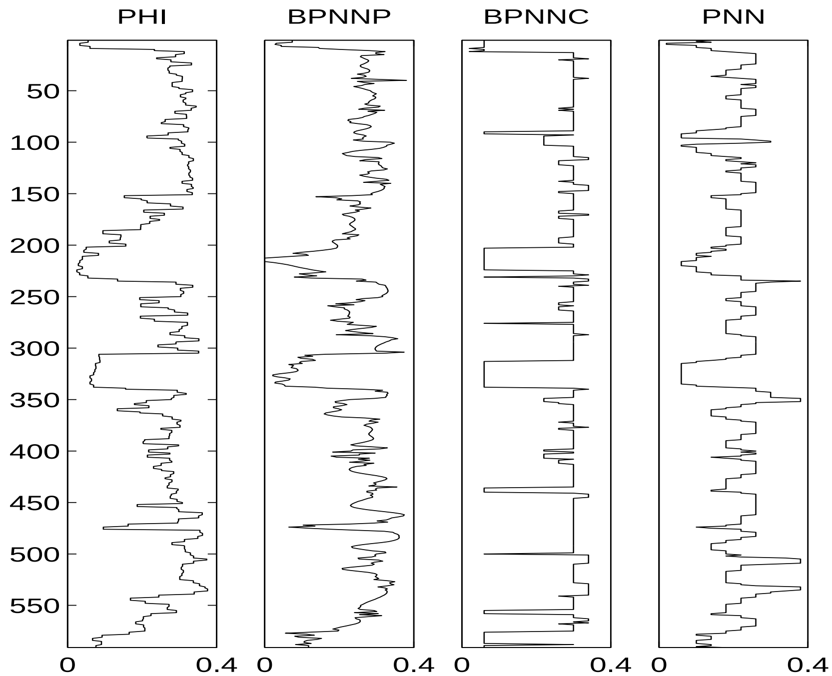

FIG. 21. ϕ predicted from five seismic attributes, using the BPNNp, BPNNc and PNN. Prediction on training data from wells 58c and 58cst. Vertical coordinates are in samples.

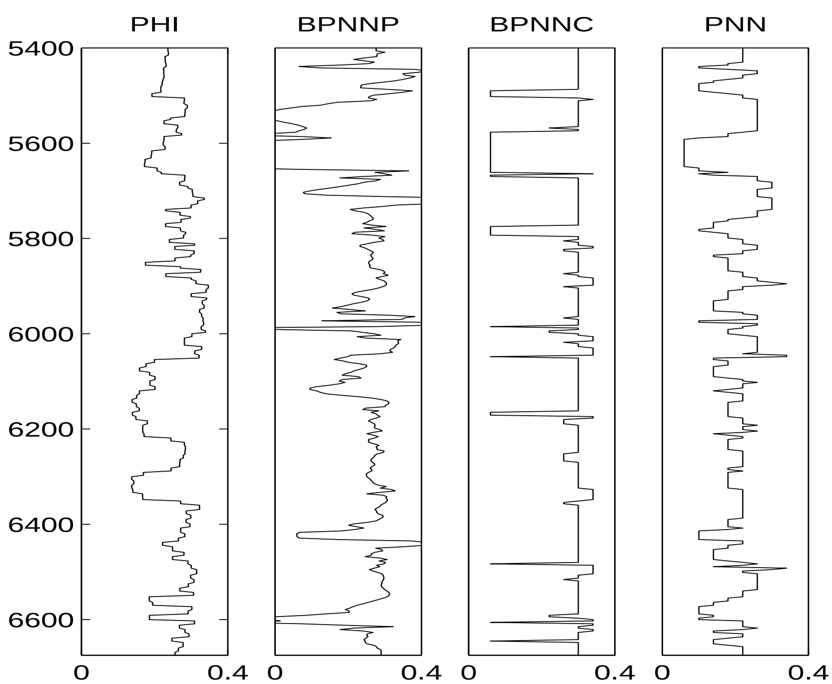

FIG. 22. ϕ predicted from five seismic attributes, using the BPNNp, BPNNc and PNN. Prediction on test data from well 56c. Vertical coordinates are in measured depth.

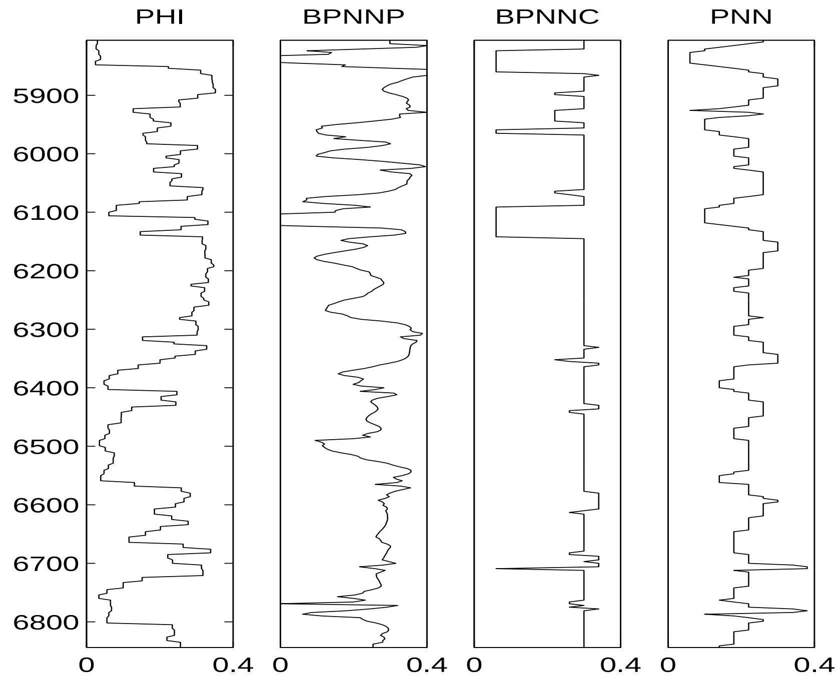

FIG. 23. ϕ predicted from five seismic attributes, using the BPNNp, BPNNc and PNN. Prediction on test data from well 55a. Vertical coordinates are in measured depth.

Seismic inversion versus seismic attributes prediction of porosity

The experiments described in the previous sections show that porosity can be predicted with a smaller rms error and higher correlation from elastic parameters as compared to predicted from seismic attributes. The gain in correlation between predicted and targeted porosity, achieved when using the elastic properties (ρ,Z_p,Z_s) as predictor instead of seismic attributes, is represented graphically in Figure 24.

In general, the correlation gain is at least 30% for the test data and tends to rise as the number of attributes used to predict porosity increases. In opposition, the correlation gain drops, but remains positive, for the training data as the number of attributes increases. Such a behavior is characteristic of the lower correlation existing between seismic attributes and porosity. Increasing the number of attributes used to train the network, increases its degree of freedom, and yields a better fit with smaller training errors. The resulting underdetermined system affects the network's generalization capabilities.

Because of their relatively high correlation with porosity, the number of elastic properties used to train the network can be keep small, maintaining an over determined network. Therefore, the network performs reliable predictions on the test data.

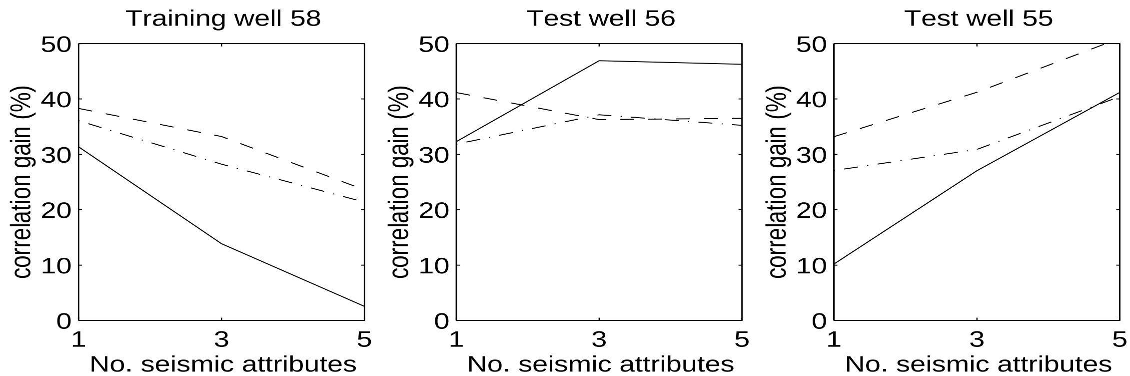

(a) (b) (c)

FIG. 24. Gain in prediction-target correlation when predicting porosity from three elastic parameters (ρ,Z_p,Z_s) versus prediction from one to five seismic attributes, realized using BPNNp (solid line), BPNNc (dashed line) and PNN (dotted line). (a) gain at the training well 58, (b) at the test well 56c, and (c) at the test well 55a.

The corresponding correlation gain achieved when Z_p alone is used to predict porosity (Figure 25), drops by 15 to 20% on the training data. Building a BPNNp with a single input (Z_p), instead of three (ρ,Z_p,Z_s), reduces its weights number from 86 to 36. With a single input neuron, and consequently half the number of network parameters, the network does not match the training data as well as with three input neurons. Nevertheless, generalization capabilities of the network are little affected when Z_p is the only predictor, since correlation gain remains mostly superior to 25% on the test data.

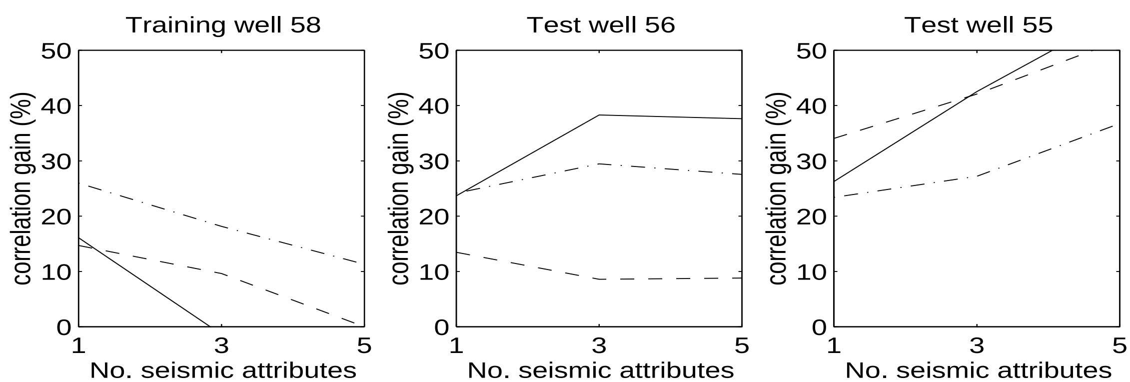

(a) (b) (c)

FIG. 25. Gain in prediction-target correlation when predicting porosity from ρ only versus prediction from one to five seismic attributes, realized using BPNNp (solid line), BPNNc (dashed line) and PNN (dotted line). (a) gain at the training well 58, (b) at the test well 56c, and (c) at the test well 55a.

The relative performance of the different competing networks is illustrated in Figure

26 which shows the prediction-target correlation gain achieved by the PNN over the BPNNp and BPNNc, when porosity is predicted from one to three elastic parameters. As described in (Ecoublet and Symes, 1997), the smoothing coefficients σ, constituting the terms of the diagonal covariance matrix Σ which defines the shape of the class-conditional probability density $p(\mathbf{X}|\theta_k)$, are computed from the data X to classify. We recall that by definition, a very small Σ would result in a perfect classification of the training data, i.e. with 100% correlation, at the expense of failing to classify some new data. Despite the PNN classification of the training data is not as effective as the BPNN classification, i.e. mostly negative gain, the PNN has predicted porosity of the test data in any case with an higher accuracy than the BPNN, i.e. gain always positive. The PNN performed an averaged 15% correlation gain over the BPNN in its classification version.

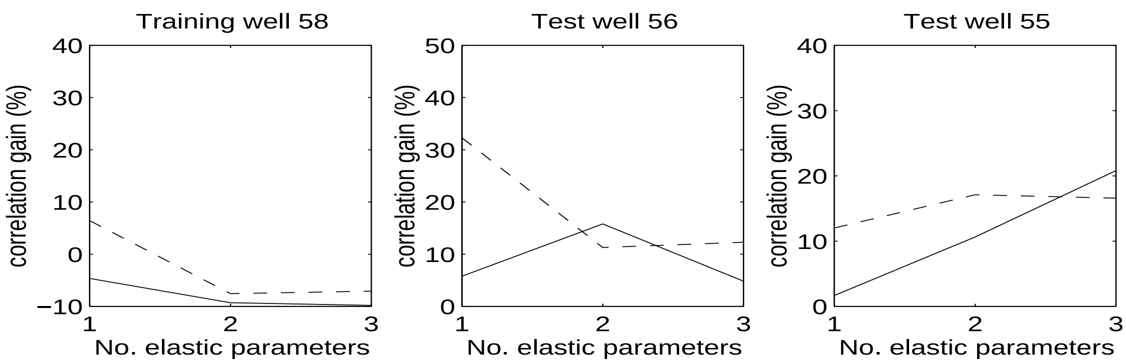

(a) (b) (c)

FIG. 26. Gain in prediction-target correlation realized by the PNN versus BPNNp (solid line), and versus BPNNc (dashed line), when predicting porosity from one (ρ), two (Z_p,Z_s), and three (ρ,Z_p,Z_s) elastic parameters. (a) gain at the training well 58, (b) at the test well 56c, and (c) at the test well 55a.

Conclusion

The study conducted on synthetic data and presented in this report demonstrates that porosity can be inferred with an higher accuracy from seismic inversion as an alternative to prediction from seismic attributes. The gain of prediction-target correlation generally exceeds 30%.

The larger prediction errors observed when predicting porosity from seismic attributes reflect the lower correlation observed between these attributes and porosity. Results show that inverted acoustic impedance alone is a good predictor of porosity. The knowledge of inverted density does not considerably improve the prediction accuracy.

The systematic comparison of results obtained with the different neural networks confirms the superiority of the probabilistic network compared to the backpropagation network. The probabilistic network allowed for an improvement of 10 to 20% of the prediction-target correlation on the test data compared to the performance of the back-propagation network.

REFERENCES

Bishop, C. M., 1996, *Neural Networks for Pattern Recognition*: Oxford, Clarendon Press.

Ecoublet, P., Symes, W. W., and Levin, S., 1997, Seismic Inversion for Porosity using a Backpropagation Neural Network: *TRIP Annual Report 97*, Rice University.

Ecoublet, P., and Symes, W. W., 1997, Application of Probabilistic Neural Network to Porosity Prediction: *TRIP Internal Report*, Rice University.

Taner M. T., Koehler, F., and Sheriff, R. E., 1979, Complex seismic trace analysis: *Geophysics*, 44:1041-1063.